Hydrogen photoproduction on TiO_2-reduced graphene oxide hybrid materials from water-ethanol mixture

Jarosław Serafin[1*], Ewelina Kusiak-Nejman[2*], Agnieszka Wanag[2], Antoni W. Morawski[2], Jordi Llorca[1]

[1]*Institute of Energy Technologies, Department of Chemical Engineering and Barcelona Research Center in Multiscale Science and Engineering, Universitat Politècnica de Catalunya, EEBE, Eduard Maristany 10-14, 08019 Barcelona, Spain*

[2]*Department of Chemical and Environment Engineering, Faculty of Chemical Technology and Engineering, West Pomeranian University of Technology, Pulaskiego 10, 70-322Szczecin, Poland*

*Coresponding author.

E-mail address: **jaroslaw.serafin@upc.edu** (J. Serafin); **ewelina.kusiak@zut.edu.pl** (E. Kusiak-Nejman)

Keywords: titanium dioxide, reduced graphene oxide, photocatalyst, hydrogen production

Abstract:

Titanium dioxide mixed with reduced graphene oxide (rGO) has been tested in the photoproduction of hydrogen using UV light from water-ethanol combination in gas phase. The presence of the reduced graphene oxide in TiO_2/rGO nanocomposites affects the physicochemical properties of hybrid materials, thus enhancing the photocatalytic activity. The obtained catalysts have been characterized for physical-chemical properties using X-ray diffraction (XRD), UV-vis spectroscopy, Raman spectroscopy, transmission electron microscopy (TEM)/high-resolution transmission electron microscopy (HRTEM), and Brauner Emmett Teller (BET). The best

photocatalyst has been obtained by mixing anatase and rGO (10 wt.%) after calcination at 700 °C. This TiO_2-rGO composite exhibited the highest performance with a hydrogen photogeneration rate of 9.5 mmol h^{-1} g^{-1}.

Keywords: Hydrogen production, photocatalysis, photoreactor, titanium dioxide, rGO

Introduction

Nowadays, fossil energy resources are principally used to meet most of the global energy needs. Current energy consumption data suggests that soon, there will be significant problems and challenges related to energy supply and demand. Combustion of fossil fuels provide to emissions of carbon particles, CO_2 and harmful gases such as SO_x and NO_x to the atmosphere [1,2]. Therefore, environmentally friendly fuels, which are both easy to store and cost-effective, are of huge significance for sustainable development [3]. Hydrogen is an perfect candidate as an energy carrier [4]. Currently, various of technologies are used to production of hydrogen. However, only a small group of them can be recognized as environmentally friendly. Hydrogen production by steam reforming of hydrocarbons (natural gas) is a dominant technology, but this technology requires high temperatures (700-1100°C) and emits large amounts of CO_2 [5]. For this reason, water splitting using light is one of the most interesting advances to hydrogen production. The water separation process can be carried out at an ambient temperature and pressure conditions, and what is most important is environmentally friendly. When higher alcohols are used as sacrificial agents, H_2 production can also be associated with the production of high value products (i.e. acetaldehyde) derived from selective alcohol oxidation [6,7]. Among various semiconductors,

TiO_2 has been extensively investigated due to its photosensitivity, chemical and thermal stability, low toxicity, and finally low cost. However, there are some limitations of its applications, it has a large band gap (about 3.2 eV for anatase), which makes it sensitive only to light below 387 nm in the ultraviolet (UV) range, and high recombination rate of electron-hole pairs [8,9]. Attempts have been made to fine tune the conduction band and/or valence band to shorten the band gap [10,11]. Another way to facilitate charge separation is to couple TiO_2 with another conductor. Graphene, as a two-dimensional sp^2 carbon network arranged in a honeycomb structure, is one of the most commonly used materials in recent years for that purpose. It has unique mechanical, optical, electronic and catalytic properties [12,13]. Composite materials containing TiO_2 and graphene may demonstrate increased photocatalytic activity due to very good mobility of electrons in the excited state, which hinders electron-hole recombination. There are many reports in the literature on various photocatalysts based on reduced graphene oxide (rGO) with TiO_2, CdS, WO_3, $BiVO_4$, ZnO [14,15,16,17,18,19,20]. Particular attention is focus to the graphene-TiO_2 nanocomposite. Sun et al. [21] synthesized graphene/TiO_2 nanocomposites by simply covering the functionalized graphene with P25 nanoparticles by heterogeneous coagulation. Li et al. [22] reported a novel Au@CdS/RGO/TiO_2 heterostructure as photoelectrode for photoelectrochemical (PEC) hydrogen generation via splitting water. Moon et al. [23] develop not only organic-electron-donor-free, but also noble-metal-free TiO_2-based photocatalytic system for the generation of H_2O_2; in-situ formation of cobalt phosphate (CoP) was achieved on the reduced graphene oxide (rGO)/TiO_2 composite. Mou et al. [24] reported N-doped graphene (NGR) composite photocatalysts (NGR/TiO_2) for solar energy conversion. Liu et al. [25] develop a facile method to synthesize TiO_2–graphene composites with different exposed crystal facets for hydrogen production. Liu H., et al. [26] prepared RGO/TiO_2 nanocomposites which were synthesized by a straightforward

procedure using $TiCl_3$ as both reducing agent to reduce GO and the precursor of TiO_2 for photocatalytic hydrogen production. The photocatalytic effect of reduced graphene oxide, despite many studies, is still the subject of many new studies because of the complexity of the rGO structure (hybridized atoms, variety of functional groups, defects, etc.). The idea of a composite with rGO allows increasing the photocatalytic efficiency because both the specific reaction sites and the photo-corresponding range are improved.

This work shows a facile method to obtain TiO_2–rGO composite photocatalysts by a hydrothermal method and investigation of the effect of calcination temperature on hydrogen's photoproduction. These composites exhibit better hydrogen photoproduction activity than TiO_2.

2. Experimental

2.1. Materials and reagents

Photocatalysts were obtained by mixing reduced graphene oxide and titanium dioxide, which was provided by Grupa Azoty Zakłady Chemiczne “Police” S.A. company (Poland) as a crude titanium dioxide slurry. A solution of ammonia (25%, Avantor Performance Materials Poland S.A.) was added to the crude slurry until pH=6.8 and dried at 105°C for 24 h. This material was denoted as starting-TiO_2. The reduced graphene oxide (rGO) was supplied by NANOMATERIALS LS (Poland) and was prepared by a modified Hummer’s method. Isopropanol (purity 99.5%) was purchased from Firma Chempur (Poland).

2.2 Synthesis of the photocatalysts

Photocatalysts containing graphene oxide and TiO_2 were synthesized by a hydrothermal method and calcined in Ar to avoid the oxidation of rGO [27,28]. Initially, 2 g of starting-TiO_2

and rGO (10 wt. %) were mechanically mixed in a mortar. The material was transferred to an autoclave containing 2 mL of isopropanol. The mixture was heated at 180°C for 4 h under autogenous pressure. To remove residual alcohol and water, the pressure valve in the reactor was open and the sample was heated for 1 h. Finally, the material was calcined at 300, 500, 700 and 900°C for 4 h under Ar flow (60 mL/min). The resulting photocatalyst were designed as TiO_2/rGO-10-300, TiO_2/rGO-10-500, TiO_2/rGO-10-700 and TiO_2/rGO-10-900. Reference samples were obtained following exactly the same method, but without rGO (denoted as TiO_2, TiO_2-500 and TiO_2-700 before calcination and after calcination at 500 and 700 °C, respectively).

2.3. Characterization methods

The phase composition and the crystalline structure of the photocatalysts were characterized by X-ray diffraction (XRD) with a PANalytical Empyrean X-ray diffractometer using Cu Kα radiation (λ=1.54056 Å). The average crystallite size was calculated according to the Scherrer's equation. Titania anatase over rutile ratio was estimated following the method described elsewhere [29]. The identification of anatase and rutile phases was based on JCPDS 01-070-7348 and 01-076-0318 standard cards, respectively. Diffuse absorbance UV-vis spectroscopy was acquired on a JASCO V-650 spectrophotometer equipped with a PIV-756 integrating sphere. Barium sulphate was used as standard. The bandgap (E_g) was determined from Tauc graphs by plotting $[F(R)\mathrm{h}v]^{1/2}$ as a function of hυ and extrapolating the linear portion to $[F(R)hv]^{1/2} = 0$ [30]. The surface area (S_{BET}) and porous structure of the photocatalysts were determined by nitrogen adsorption-desorption measurements at 77 K on a QUADRASORB evo™ Gas Sorption analyzer. Prior to measurements, the samples were degassed at 100°C for 12 h under vacuum. The surface area (S_{BET}) was calculated by the multipoint Brunauer-Emmett-Teller (BET) method, while the total pore volume (V_{total}) was determined on the basis of the adsorbed N_2 at a relative pressure

p/p_0=0.99.The micropore volume ($V_{microDR}$) was calculated by applying the Dubinin-Radushkevich (DR) equation using adsorption branches of the measured isotherm. The mesopore volume (V_{meso}) was calculated by subtracting micropore volume from the total pore volume. Raman spectra were collected with a Renishaw in Via Qontor confocal Raman microscope equipped with a 532.1± 0.3 nm laser with a nominal 100 mW output power directed through a specially adapted Leica DM2700 M microscope (x50 magnification). Spectra were acquired in the two ranges, 50-800 cm^{-1} and 1000-2000 cm^{-1}, with an exposure time of 0.5 s, 1% of maximum laser power and 18 repetitions. Total carbon content was determined using a CN 628 elemental analyzer (LECO Corporation, USA). Transmission electron microscopy analysis (HRTEM and HAADF-STEM) was carried out using a FEI Tecnai F20 electron microscope equipped with a field emission electron gun operating at 200 kV. The samples were prepared by dispersing the powder catalysts in an alcohol suspension; a drop of the dispersion was placed over a grid with a lacey-carbon film.

2.4. Photocatalytic hydrogen production

To perform the photocatalytic tests were use a tubular glass photoreactor (Figure S1). The analyses were made at 25°C and atmospheric pressure under dynamic conditions. Gaseous reactant mixture of H2O: EtOH=9:1 on a molar basis, which was directly introduced in the photoreactor, was obtained with an argon stream (20 mL/min) bubbled through a Drechsel bottle containing a liquid mixture of water-ethanol. The partial pressure of ethanol was 0.30 kPa. An UV light source from SACOPA S.A.U. consisting of four LEDs emitting at 365±5 nm and a synthetic quartz cylindrical lens that transmitted the light to the photocatalyst was used [31,32]. The photocatalyst samples (2 mg) were dispersed in ethanol and ultrasonicated and the resultant suspension was placed onto circular porous cellulose membranes (from AlbetLabScience, pore size 35-40 µm, 80

g/m^2, thickness 0.18 mm). The sizes of membrane surface covered by the photocatalyst was 1.88 cm^{-2}. The impregnated cellulose membranes were dried at 60ºC, weighted to check for the amount of supported photocatalyst and then placed in the photoreactor. The gas hourly space velocity (GHSV) was ca. 100,000 h^{-1}. The irradiance over the sample was 80±2 mW/cm^2 as measured with a UV-A sensor (model PMA 2110, Solar Light Co.), which registered the UV radiation within spectral response 320-400 nm, connected to a radiometer (model PMA2200, Solar Light Co.). The outlet of the photoreactor was directly connected to a Varian CP-4900gas chromatograph (GC) equipped with MS 5 Å, Plot U and Stabilwax columns for a complete analysis of the photoreaction products, which were monitored on-line every 4 minutes.

The apparent quantum yield (AQY) was calculated using equation:

$$\mathrm{AQY} = \frac{2n_{H2}}{n_p} \cdot 100 = \frac{nN_A}{E_T/E_P} \cdot 100$$

Where n_{H2} is the number of molecules of H_2 generated and n_p is the number of incident photons reaching the catalyst. The number of incident photons can be calculated by $np= E_T/E_p$, where E_T is the total energy reaching the catalyst and E_p is the energy of a photon.

E_T=PSt, where P (W m^2) is the power density of the incident monochromatic light, S (m^2) is the irradiation area and t(s) is the duration of the incident light exposure. E_p=hc/λ, where h is the Planck's constant, c the speed of light and λ (m) is the wavelength of the incident monochromatic light. The number of hydrogen molecules can be calculated as n_{H2}=nN_A, where n are H_2 moles evolved during the time of light exposure (t), and N_A is the Avogadro constant [33]. In our case, experimental conditions were: the wavelength of the incident light was λ = 365 nm, the power density of the incident light at the paper surface was P=80 mW cm^2 and the irradiation area was S=1.88 cm^2.

3. Results and discussion

3.1. Characterization of the samples

The XRD profiles of the samples prepared in this work are presented in Figure 1. Table 1 lists the crystalline phase composition and the average crystallite size of anatase and rutile phases.

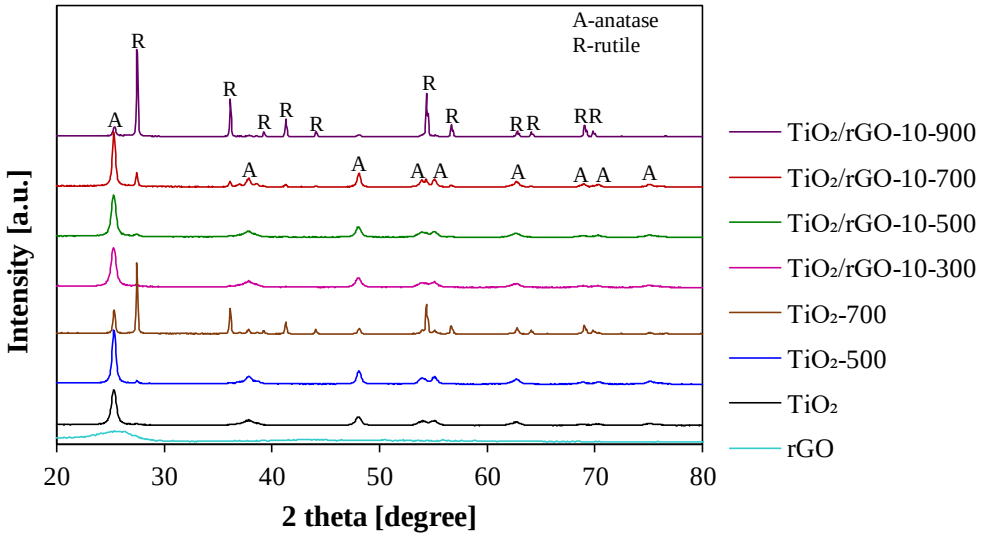

Fig. 1. XRD patterns of the samples prepared in this work.

Table 1. Phase composition and crystallite size (d) of the samples prepared in this work.

Sample	Crystalline phase concentration[%]		Anatase	Rutile
	Anatase	Rutile	d_A [nm]	d_R [nm]
TiO_2	98	2	18	33
TiO_2/rGO-10-300	98	2	19	27
TiO_2-500	98	2	26	47
TiO_2/rGO-10-500	98	2	21	28
TiO_2-700	28	72	58	>100
TiO_2/rGO-10-700	84	16	35	>100
TiO_2/rGO-10-900	14	86	42	>100

The sample TiO_2 used as precursor primarily consists of anatase phase (98%) with a negligible fraction of the rutile phase, according to previous reports**.** The XRD patterns for rGO-modified TiO_2 did not show peaks corresponding to graphene. This has also been observed in our previous works [34,35,36] and it is related to the small amount of rGO with relatively low diffraction intensity [37] and also to the overlapping of the main rGO peak at 24.2° with that of anatase at 25.4° [38]. The appearance of rutile at the expense of anatase generally occurs at calcination temperatures higher than ca. 500°C [39]. Above this temperature, a typical anatase-to-rutile phase transition is observed. It is interesting to note that the presence of rGO strongly inhibits the anatase-to-rutile transformation. In particular, the samples calcined at 700°C in absence and presence of rGO (TiO_2-700 and TiO_2/rGO-10-700) contain 72% and 16% of rutile phase, respectively (Table 1). Thus, the anatase phase exhibits much higher thermal stability after rGO modification, which is a direct proof of the intimate contact between rGO and TiO_2. Also, 14% of anatase phase is found for TiO_2/rGO-10 calcined at 900°C, whereas at this temperature the bare TiO_2 anatase phase fully converts to rutile [40]. This behaviour is opposite to that exhibited by TiO_2 samples doped with carbon/graphite, which are strong reducing agents and promote the anatase to rutile transformation via oxygen vacancy and defect formation [41,42]. In addition, the presence of rGO also inhibited the growth of both anatase and rutile crystallites (Table 1), again pointing out to a strong interaction between rGO and TiO_2.Therefore, the rGO flakes restrictTiO_2 phase transformation and sintering.

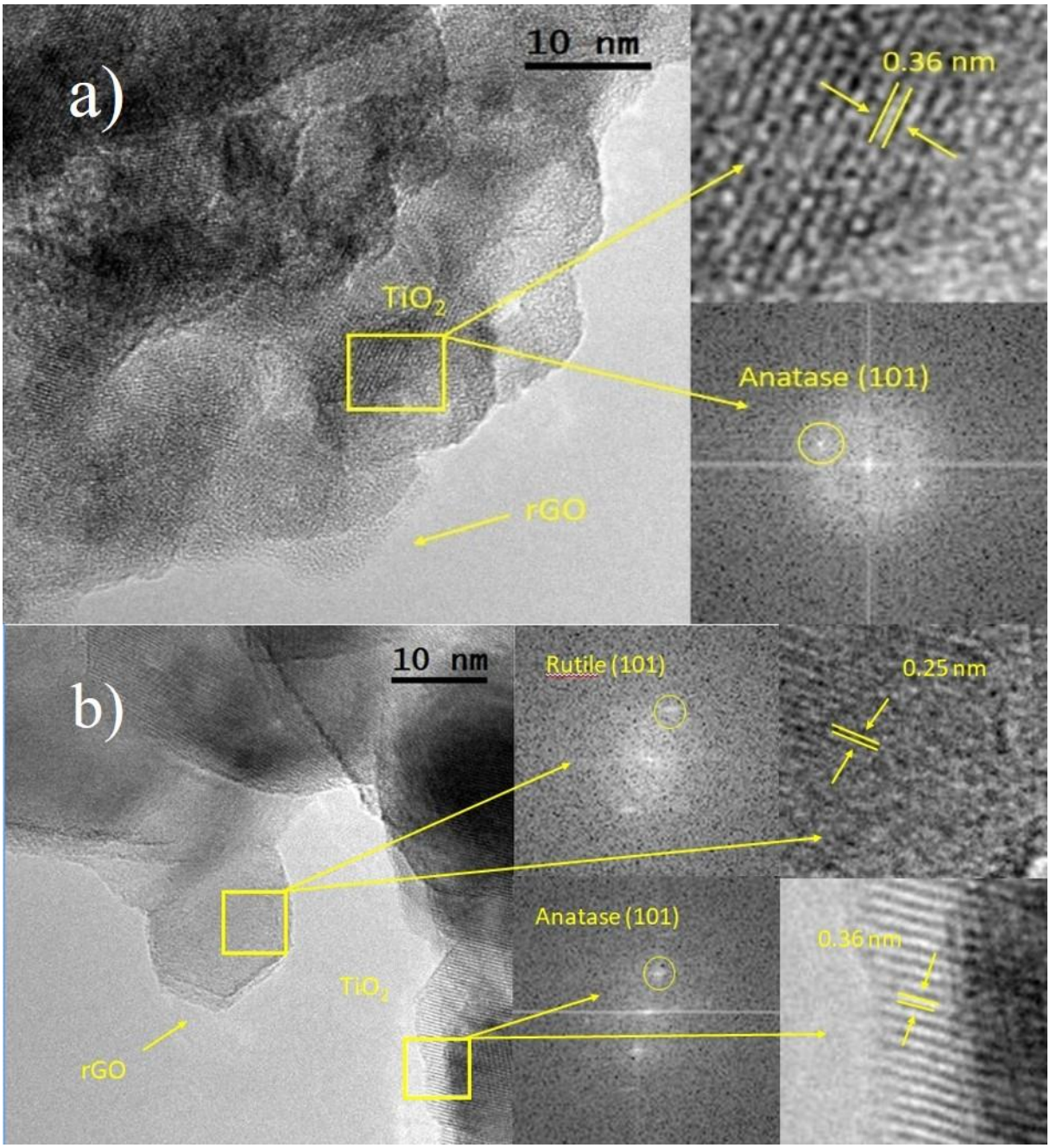

Fig. 2. TEM images of TiO_2/rGO-10-300 (a) andTiO_2/rGO-10-700 (b)

The morphology of the prepared photocatalysts TiO_2/rGO-10-300 andTiO_2/rGO-10-700 were characterized by TEM and images are shown in Figure 2. In both samples, HRTEM images showed

TiO_2 with lattice spacing of 0.36 nm, which corresponds to the anatase (101) plane. For theTiO_2/rGO-10-700 TiO_2 sample, lattice spacing of 0.25 nm corresponds to the rutile (101) plane. These results are in accordance with the XRD data presented in Table 1.

The UV-vis absorption spectra of the samples used in this work are presented in Figure 3 and the corresponding calculated band gap energy values are listed in Table 2. The TiO_2 material is characterized by high absorption in the UV region [43]. TiO_2 samples calcined at 500 and 700°C show a noticeable shift of the absorption edge into the visible region caused by the anatase-to-rutile transformation [44]; this is particularly evident for TiO_2-700. Photocatalysts modified with rGO exhibit absorption in the visible region. This absorption is caused by both the rGO content and calcination, which caused changes in samples colour. Moreover, it can be observed that the absorption increases with the increase of calcination temperature. After modification with rGO and calcination, photocatalysts changed colour from white for TiO_2-A180 to grey. The highest absorption in the visible region was noticed for the sample TiO_2/rGO-10-900. For this sample, it can also be observed a significant shift in the absorption into the visible region related to a decrease of the energy band-gap value. Estimated band gap values for all tested nanomaterials are listed in Table 2. The band gap energy for TiO_2/rGO-10-900 material is the lowest and reaches 2.95 eV (the band gap varies from 2.95 to 3.28 eV). Both shifts in the absorption into the visible region and narrowing the band gap energy are attributed to the presence of rutile in the photocatalyst [43].

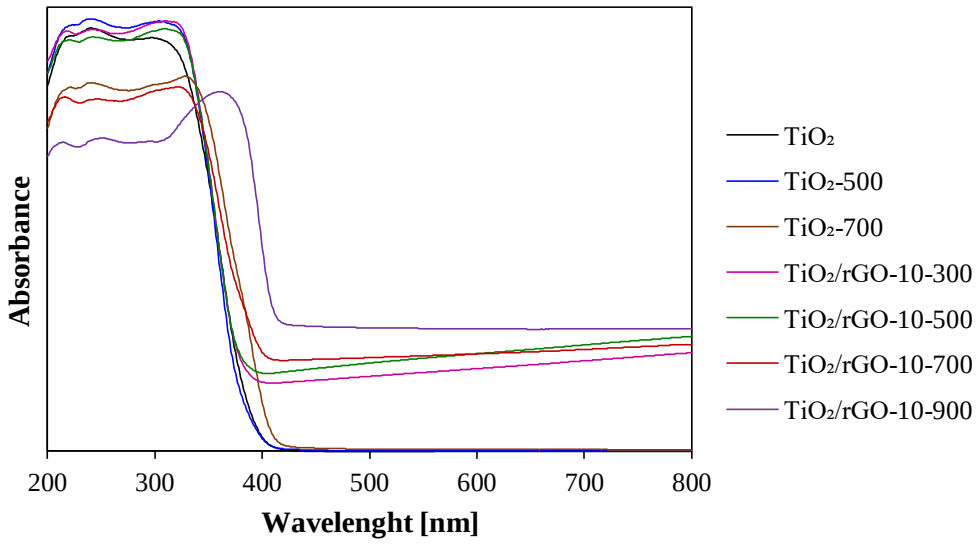

Fig. 3. UV-Vis absorbance spectra of TiO_2 and rGO- TiO_2 photocatalysts.

Table 2. Physical properties, carbon content and calculated band gap values.

Sample code	S_{BET} [m^2/g]	V_{total} [cm^3/g]	V_{micro}[cm^3/g]	V_{meso} [cm^3/g]	Carbon content[wt.%]	Eg [eV]
TiO_2	97	0.40	0.04	0.36	0.6	3.28
TiO_2/rGO-10-300	140	0.35	0.05	0.30	6.5	3.27
TiO_2/rGO-10-500	126	0.38	0.05	0.33	6.7	3.28
TiO_2-500	78	0.23	0.03	0.20	-	3.29
TiO_2/rGO-10-700	91	0.23	0.03	0.20	7.2	3.15
TiO_2-700	15	0.05	0.004	0.05	-	3.02
TiO_2/rGO-10-900	50	0.12	0.02	0.10	6.6	2.95
rGO	310	0.31	0.12	0.19	-	-

The BET surface area values and pore volumes of the nanomaterials studied in this work are listed in Table 2 as well as their carbon content determined by elemental analysis. All TiO_2-rGO materials exhibit similar carbon content, between 6.5 and 7.2 wt. %. It is noted that a mesoporous structure characterizes the photocatalysts. The calcination of TiO_2 generally led to the

decrease of the S_{BET} values and total pore volume, as expected. This is strongly related to the increase of crystallite size (see Table 1) [45]. By comparing the results obtained for rGO-decorated photocatalysts and reference TiO_2 samples, it is possible to conclude that rGO modification caused a noticeable increase of the S_{BET} surface area and total pore volume. This observation is attributed to the structural and physical properties of rGO (S_{BET}=310 m^2/g; V_{total}=0.32 cm^3/g) [46].

Figure 4 shows the Raman spectra of the rGO-TiO_2 photocatalysts. In all cases the spectra is dominated by the characteristic signals of anatase (presented in Figure 4a) and the broad D and G peaks of rGO located at ca. 1300 and 1600 cm^{-1}, respectively (Figure 4b). The typical modes of anatase could be observed: the $E_{g(1)}$ peak (148 cm^{-1}), $B_{1g(1)}$ peak (394 cm^{-1}), $E_{g(2)}$ peak (637 cm^{-1}), and the $A_{1g} + B_{1g(2)}$ modes centered at 512 cm^{-1}.No rutile peaks are visible due to their low intensity in the Raman spectra with respect to anatase. The two characteristic peaks at about 1328 and 1602 cm^{-1} for the graphitized structures were also observed in the Raman spectrum of the rGO-TiO_2 composites.The values of the G/D intensity ratio range from 0.76 to 0.86, which are characteristic of the high disorder of the rGO structure [47].

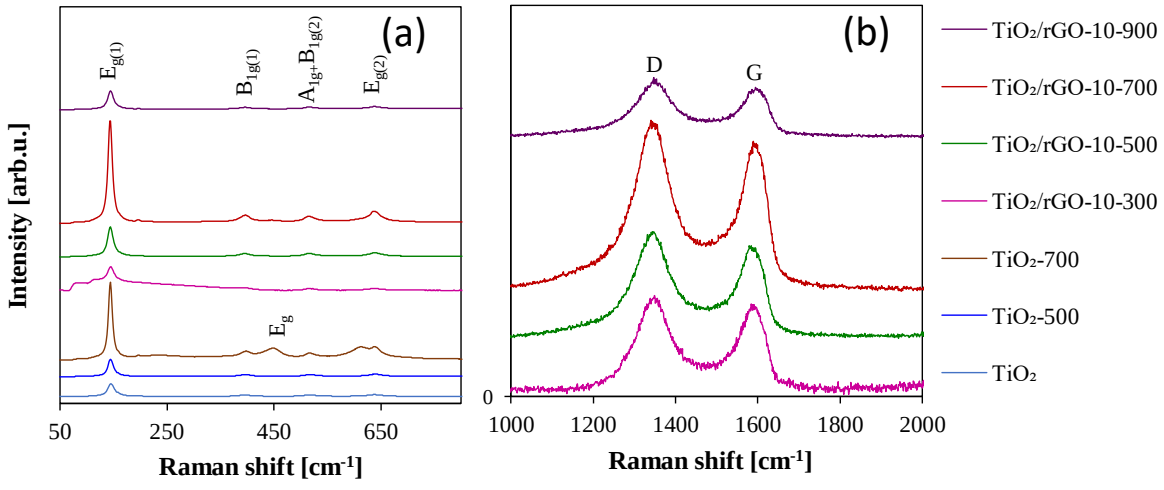

Fig. 4. Raman spectra of rGO-TiO_2 photocatalysts.

3.2. Photoproduction of hydrogen

The samples were tested in the photogeneration of hydrogen at atmospheric pressure using a gas EtOH:H_2O mixture (10% EtOH, molar) at room temperature (25°C) at a gas hourly space velocity of GHSV=100,000 h^{-1}. Steady-state normalized hydrogen photogeneration rates are shown in Figure 5. It can be easily seen that the photoproduction of hydrogen is higher for the photocatalysts modified with rGO than for reference samples without rGO. The reference samples TiO_2, TiO_2-500 and TiO_2-700 produced smaller amounts of hydrogen comparing with samples modified with rGO; almost an order of magnitude. Therefore, a significant increase in the photogeneration of hydrogen is associated with the combination of titanium dioxide with rGO (Figure S2). Importantly, the production of hydrogen was stable over time. Reduced GO promotes electron mobility and decreases charge carrier recombination rate. The photogenerated electrons migrate from the TiO_2 to rGO, improving the photoactivity [48]. The calcination temperature during the preparation of the photocatalysts has a strong effect on the photoproduction of hydrogen in the rGO-TiO_2 samples. The phase composition of photocatalyst is one of the most crucial parameter that affects photoactivity. It is commonly known that samples consisting mainly of the anatase phase show higher activity than samples contain rutile [49]. Accordingly, the TiO_2-700 and TiO_2/rGO-10-900 samples containing 72 and 86% of rutile, respectively, shows definitely lower hydrogen production. The most substantial effect is observed for TiO_2/rGO-10-700 photocatalyst consisting of 84 and 16% of anatase and rutile, respectively. A similar phase content is encountered in the commercial photocatalyst AEROXIDE® TiO_2 P25, which is considered the standard photocatalyst. It has been demonstrated that such proportion of anatase to rutile is related to better charge carriers separation and higher activity [50]. Both effects, rGO modification and calcination process benefit the photocatalytic efficiency of the material. The apparent quantum yield (AQY) of TiO_2-rGO-700, calculated as described in the Section 2.4., was 2.24%, notably above the 0.18% estimated for pure TiO_2 (Table S1).

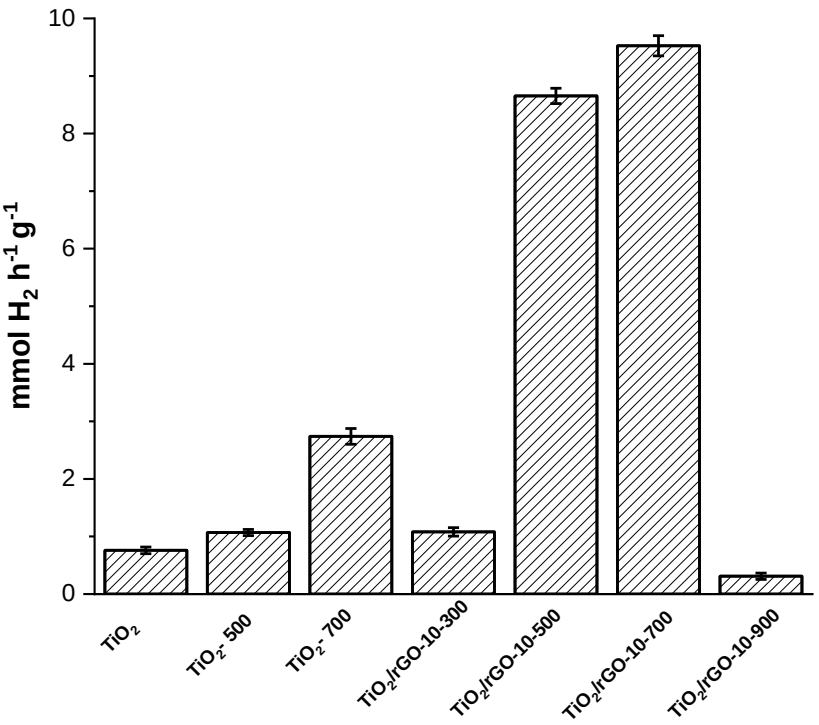

Fig. 5. Hydrogen photoproduction rates recorded at 25°C, EtOH:H_2O=1:9 (molar) and GHSV=100,000 h^{-1}(0.036 s contact time).

The production of hydrogen using titanium dioxide has been the subject of many studies. The summary of recent representative studies described in the literature carried out on TiO_2 composites and the results of this study are shown in Table 3. The catalysts prepared in this work show H_2 photoproduction rates which are among the highest ever reported in the literature, competing only with nitrogen-doped TiO_2-C_3N_4 composites.

The production of hydrogen using titanium dioxide has been the subject of many studies. The summary of recent representative studies described in the literature carried out on TiO_2 composites, and the results of this study are shown in Table 3. One can notice a significant increase in the

photoproduction of composite hydrogen to titanium oxide alone. Titanium dioxide without the addition of rGO produced smaller amounts of hydrogen concerning the samples modified with rGO. Similar conclusions get Chen et al. [51] when investigating commercial titanium oxide and titanium oxide doped with Au. Also, Xing et al. [52] under similar conditions achieved hydrogen production for TiO_2 and $NiTiO_3$ / TiO_2: 3 mmol h^{-1} g^{-1}, 11.5 mmol h^{-1} g^{-1}, respectively. The catalysts prepared in this work show H_2 photoproduction rates, one of the highest among ever reported in the literature, competing only with nitrogen-doped TiO_2-C_3N_4 composites.

Table 3. H_2 production rates reported for titanium dioxide composites in the literature and H_2 production rates obtained in this work.

Catalyst	**Light source**	**Electron donor**	**Light intensity (mW· cm^{-2})**	**H_2 production ($mmol \cdot h^{-1} \cdot g^{-1}$)**	**Ref.**
TiO_2/rGO	UV-Vis	Methanol[l]	NA	0.74	53
TiO_2/rGO	>320	Methanol[l]	205	NA	54
g-C_3N_4/N[a]-TiO_2nanofibres	Xe lamp	Methanol[l]	NA	8.93	55
W/N[b]-TiO_2	Vis	Ethanol[l]	NA	0.018	56
C[c]-TiO_2/rGO	Xe lamp	Methanol[l]	135	1.5	57
C-TiO_2	Xe lamp	TEOA[f,l]	135	0.049	57
C-TiO_2-rGO	Xe lamp	TEOA[l]	135	0.066	57
TiO_2/G[d]	UV-Vis	Na_2S/Na_2SO_3[l]	80	0.108	58
N[e]-TiO_2/N[e]-GO	Hg lamp	Methanol[l]	NA	0.996	59
TiO_2 P90	UV	Water-Ethanol[g]	87±0.5	1.5	51
Au/P90-BM	UV	Water-Ethanol[g]	87±0.5	49.3	51
TiO_2	UV	Water-Ethanol[g]	79.1±0.5	3.0	52
$NiTiO_3$/TiO_2	UV	Water-Ethanol[g]	79.1±0.5	11.5	52
TiO_2	UV	Water-Ethanol[g]	80	0.76	This study
TiO_2- 500	UV	Water-Ethanol[g]	80	1.07	This study
TiO_2- 700	UV	Water-Ethanol[g]	80	2.74	This study
TiO_2-rGO-10-500	UV	Water-Ethanol[g]	80	8.66	This study
TiO_2-rGO-10-700	UV	Water-Ethanol[g]	80	9.53	This study

[1] J. Serafin, U. Narkiewicz, A.W. Morawski, R.J. Wrobel, B. Michalkiewicz, Highly microporous activated carbons from biomass for CO_2 capture and effective micropores at different conditions. J. of CO_2 Util. 18 (2017) 73-79.doi.org/10.1016/j.jcou.2017.01.006.

[2] J. Serafin, M. Baca, M. Biegun, E. Mijowska, R. J. Kaleńczuk, J. Sreńscek-Nazzal, B. Michalkiewicz, Direct conversion of biomass to nanoporous activated biocarbons for high CO_2 adsorption and supercapacitor applications. Appl. Surf. Sci. 497 (2019) 143722., doi.org/10.1016/j.apsusc.2019.143722.

[3] S. Mao, S. Shen, L. Guo, Nanomaterials for renewable hydrogen production, storage and utilization. Progress in Natural Science: Materials International, 22 (2012) 522-534., doi.org/10.1016/j.pnsc.2012.12.003.

[4] D. Jing, L. Guo, L. Zhao, X. Zhang, H. Liu, M. Li, S. Shen, G. Liu, X. Hu, Efficient solar hydrogen production by photocatalytic water splitting: From fundamental study to pilot demonstration, Int. J. Hydrogen Energ., 35 (2010) 7087-7097.,doi.org/10.1016/j.ijhydene.2010.01.030.

[5] P. Häussinger, R. Lohmüller, A. Watson, Hydrogen, 1. Properties and Occurence.Ullmann's Encyclopedia of Industrial Chemistry. 2011.

[6] Y. Navarro, M. Rufino,.M.C. Álvarez-Galván, F. Del Valle, F., J.A. Villoria De La Mano, J.L.G. Fierro, Water Splitting on Semiconductor Catalysts under Visible-Light Irradiation, ChemSusChem, 2 (2009) 471-485., doi.org/10.1002/cssc.200900018

[7] K. Maeda, K. Teramura, D. Lu, T. Takata, S. Inoue, K. Domen, Photocatalyst releasing hydrogen from water, Nature, 440 (2006) 295., doi: 10.1038/440295a.

[8] H. Chen, C.E. Nanayakkara, V. H. Grassian, Titanium dioxide photocatalysis in atmospheric chemistry, Chem. Rev. 112 (2012) 5919- 5948., doi.org/10.1021/cr3002092.

[9] L. Wang, T. Sasaki, Titanium oxide nanosheets: graphene analogues with versatile functionalities,Chem. Rev. 114 (2014) 9455- 9486., doi: 10.1021/cr400627u.

[10] G.I.N. Waterhouse, A.K. Wahab, M. Al-Oufi, V. Jovic, D.H. Anjum, D. SunWaterhouse, J. Llorca, H. Idriss, Hydrogen production by tuning the photonic band gap with the electronic band gap of TiO_2, Sci. Rep., 3 (2013) 2849–2853., doi: 10.1038/srep02849.

[11] X. Zheng, S. Meng, J. Chen, J. Wang, J. Xian, Y. Shao, X. Fu, D. Li, Titanium Dioxide Photonic Crystals with Enhanced Photocatalytic Activity: Matching Photonic Band Gaps of TiO_2 to the Absorption Peaks of Dyes, J. Phys. Chem. C, 117(2013) 21263–21273., doi: 10.1021/jp404519j.

[12] A. Cao, Z. Liu, S. Chu, M. Wu, Z. Ye, Z. Cai, Y. L. Chang, S.F. WangQ. H. Gong, Y. F. Liu, A facile one-step method to produce graphene CdS quantum dot nanocomposites as promising optoelectronic materials,Adv. Mater. 22(2010) 103-106., doi: 10.1002/adma.200901920.

[13] Q. Li, B. D. Guo, J. G. Yu, J.G. Ran, B.H. Zhang H.J. Yan J. R. Gong, Highly efficient visible-light-driven photocatalytic hydrogen production of CdS-cluster-decorated graphene nanosheets, J. Am. Chem. Soc. 133 (2011) 10878-10884., doi.org/10.1021/ja2025454.

[14] Q. Xiang, J. Yu, M. Jaroniec, Synergetic effect of MoS_2 and graphene as cocatalysts for enhanced photocatalytic H_2 production activity of TiO_2 nanoparticles. J. Am. Chem. Soc. 134 (2012) 6575–6578., doi.org/10.1021/ja302846n

[15] W. Fan, Q. Lai, Q. Zhang, Y. Wang, Nanocomposites of TiO_2 and reduced graphene oxide as efficient photocatalysts for hydrogen evolution. J. Phys. Chem. C, 115 (2011) 10694–10701., doi.org/10.1021/jp2008804

[16] Q. Xiang, J. Yu, M. Jaroniec, Graphene-based semiconductor photocatalysts, Chem. Soc. Rev., 41 (2012) 782–796., doi.org/10.1039/C1CS15172J

[17] M. Higashi, R. Abe, T. Takata, and K. Domen, Photocatalytic Overall Water Splitting under Visible Light Using $ATaO_2N$ (A = Ca, Sr, Ba) and WO_3in a IO_3^-/I^-Shuttle Redox Mediated System, Chem. Mater., 21 8 (2009) 1543-1549., doi.org/10.1021/cm803145n

[18] Y. Wang, W. Wang, H. Mao, Y. Lu, J. Lu, J. Huang, Z. Ye, B. Liu, Electrostatic self-assembly of $BiVO_4$-reduced graphene oxide nanocomposites for highly efficient visible light photocatalytic activities, ACS Appl. Mater. Inter. 6 (2014) 12698–12706., doi.org/10.1021/am502700p

[19] A. Iwase, Y. Ishiguro, A. Kudo, R. Amal, Reduced graphene oxide as a solid-state electron mediator in Z-scheme photocatalytic water splitting under visible light, J. Am. Chem. Soc., 133 (2011) 11054-11057., doi.org/10.1021/ja203296z

[20] M. J. Sampaio, C. G. Silva, R. R. N. Marques, A. M. T. Silva, and J. L. Faria, Carbon nanotube–TiO_2 thin films for photocatalytic applications, Catal. Today, 161 1 (2011) 91-96., doi.org/10.1016/j.cattod.2010.11.081

[21] S. Sun L. Gao, Y. Liu, Enhanced dye-sensitized solar cell using$graphene$eTiO_2 photoanode prepared by heterogeneous coagulation, Appl Phys Lett., 96 (2010) 083113., doi.org/10.1063/1.3318466

[22] W. Fan X. Yu, H.Ch Lu, H. Bai, Ch. Zhang, W. Shi, Fabrication of TiO_2/RGO/Cu_2O heterostructure for photoelectrochemical hydrogen production. Appl. Catal. B-Environ., 181 (2016) 7-15., doi.org/10.1016/j.apcatb.2015.07.032

[23] G. H. Moon, W. Kim, A. D. Bokare, N. Sung, W. Choi, Solar production of H_2O_2 on reduced graphene oxide-TiO_2 hybrid photocatalysts consisting of earth-abundant elements only, Energy Environ. Sci., 7 (2014) 4023-4028., doi.org/10.1039/C4EE02757D

[24] Z. Mou, Y. Wiu, J. Sun, P. Yang, Y. Du, Ch. Lu, TiO_2 Nanoparticles-functionalized N-doped graphene with superior interfacial contact and enhanced charge separation for photocatalytic hydrogen generation, ACS Appl. Mater. Inter., 6 (2014) 13798–13806., doi.org/10.1021/am503244w

[25] L. Liu, Z. Liu, A. Liu, X. Gu, Ch. Ge, F. Gao, L. Dong, Engineering the TiO_2-graphene interface to enhance photocatalytic H_2 production, ChemSusChem, 7 (2014) 618-626., 10.1002/cssc.201300941

[26] H. Li, X. Cui, A hydrothermal route for constructing reduced graphene oxide/TiO_2 nanocomposites: Enhanced photocatalytic activity for hydrogen evolution, Int. J. Hydrogen Energy 39 (2014) 19877–19886., doi.org/10.1016/j.ijhydene.2014.10.010

[27] H.-H. Chun, W.-K. Jo, Adsorption and photocatalysis of 2-ethyl-1-hexanol over graphene oxide–TiO_2 hybrids post-treated under various thermal conditions, Appl. Catal. B: Environ., 180 (2016) 740-750., doi.org/10.1016/j.apcatb.2015.07.021.

[28] Y. Zhang, X. Hou, T. Sun, X. Zhao, Calcination of reduced graphene oxide decorated TiO_2 composites for recovery and reuse in photocatalytic applications, Ceram. Int. 43 (2017) 1150-1159. , doi.org/10.1016/j.ceramint.2016.10.056.

[29] G. Colón, J.M. Sánchez-España, J.M. Hidalgo, J.A. Novío, Effect of TiO_2 acidic pre-treatment on the photocatalytic properties for phenol degradation, J. Photochem. Photobiol. A: Chem. 179 (2006) 20-27., doi.org/10.1016/j.jphotochem.2005.07.007.

[30] D. Chen, L. Zou, S. Li, F. Zheng, Nanospherical like reduced graphene oxide decorated TiO_2 nanoparticles: an advanced catalyst for the hydrogen evolution reaction, Sci. Rep. 6 (2016) 20335., doi: 10.1038/srep20335.

[31] L. Martínez, M. Benito, I. Mata, L. Soler, E. Molins, J. Llorca, Preparation and photocatalytic activity of Au/TiO_2 lyogels for hydrogen production, Sustain. Energ. Fuels 2 (2018) 2284-2295., doi: 10.1039/C8SE00293B

[32] J. Serafin, L. Soler, D. Vega, A. Rodríguez, J. Llorca, Macroporous silicon coated with M/TiO_2 (M=Au,Pt) as a highly efficient photoreactor for hydrogen production, Chem. Eng. J., 393 (2020) 124701 doi.org/10.1016/j.cej.2020.124701

[33] Y. Li, P. Han, Y. Hou, S. Peng and X. Kuang, Oriented $Zn_mIn_2S_{m+3}$@In_2S_3 heterojunction with hierarchical structure for efficient photocatalytic hydrogen evolution, Appl. Catal., B, 244 (2019) 604-611., doi.org/10.1016/j.apcatb.2018.11.088

[34] A.W. Morawski, E. Kusiak-Nejman, A. Wanag, J. Kapica-Kozar, R.J. Wróbel, B. Ohtani, M. Aksienionek, L. Lipińska, Photocatalytic degradation of acetic acid in the presence of visible light-active TiO_2-reduced graphene oxide photocatalysts, Catal. Today, 280 (2017) 108-113., doi.org/10.1016/j.cattod.2016.05.055.

[35] E. Kusiak-Nejman, A. Wanag, Ł. Kowalczyk, J. Kapica-Kozar, C. Colbeau-Justin, M.G. Méndez-Medrano, A.W. Morawski, Graphene oxide-TiO_2 and reduced graphene oxide-TiO_2 nanocomposites: Insight in charge-carrier lifetime measurements, Catal. Today, 287 (2017) 189-195., doi.org/10.1016/j.cattod.2016.11.008.

[36] E. Kusiak-Nejman, A. Wanag, Ł. Kowalczyk, M. Zgrzebnicki, B. Tryba, J. Przepiórski, Methylene blue decomposition on TiO_2/reduced graphene oxide hybrid photocatalysts obtained by a two-step hydrothermal and calcination synthesis, Catal. Today, 2019, in press, doi.org/10.1016/j.cattod.2019.04.078.

[37] Y. Liu, Hydrothermal synthesis of TiO_2–RGO composites and their improved photocatalytic activity in visible light, RSC Adv., 4 (2014) 36040-36045., doi: 10.1039/C4RA06342B.

[38] X. Rong, F. Qiu, Ch. Zhang, L. Fu, Y. Wang, D. Yang, Preparation, characterization and photocatalytic application of TiO_2-graphene photocatalyst under visible light irradiation, Ceram. Int., 41 (2015) 2502-2510., doi.org/10.1016/j.ceramint.2014.10.072.

[39] S. Sheshmani, M. Nayebi, Modification of TiO_2 with graphene oxide and reduced graphene oxide; Enhancing photocatalytic activity of TiO_2 for removal of Remazol Black B, Polym. Compos., 40 (2019) 210-216., doi.org/10.1002/pc.24630.

[40] A. Ibrahim, W. Mekprasart, W. Pecharapa, Anatase/Rutile TiO_2 composite prepared via sonochemical process and their photocatalytic activity, Mater. Today: Proceedings 4 (2017) 6159-6165., doi.org/10.1016/j.matpr.2017.06.110.

[41] D.A.H. Hanaor, C.C. Sorell, Review of the anatase to rutile phase transformation, J. Mater. Sci. 46 (2011) 855-874., 10.1007/s10853-010-5113-0.

[42] D.A.H. Hanaor, M. Michelazzi, J. Chenu, C. Leonelli, C.C. Sorrell, The effects of firing conditions on the properties of electrophoretically deposited titanium dioxide films on graphite substrates, J. Eur. Ceram. Soc. 31(2011) 2877-2885., doi.org/10.1016/j.jeurceramsoc.2011.07.007.

[43] L.L. Tan, W.J. Ong, S.P. Chai, A.B. Mohamed, Reduced graphene oxide-TiO_2 nanocomposite as a promising visible-light-active photocatalyst for the conversion of carbon dioxide, Nanoscale Res. Lett. 8 (2013) 465., 10.1186/1556-276X-8-465.

[44] D. Reyes-Coronado, G. Rodriguez-Gattorno, M.E. Espinosa-Pesqueira, C. Cab, R. de Coss, G. Oskam, Phase-pure TiO_2 nanoparticles: anatase, brookite and rutile, Nanotechnol. 19 (2008) 145605-145615., doi: 10.1088/0957-4484/19/14/145605.

[45] Y.C. Wong, Y.P. Tan, Y.H. Taufiq-Yap, I. Ramli, Effect of calcination temperatures of CaO/Nb_2O_5 mixed oxides catalysts on biodiesel production, Sains Malays. 43 (2014) 783-790.

[46] M. Kim, W.H. Hong, W. Kim, S.H. Park, W.K. Jo, 2D reduced graphene oxide–titania nanocomposites synthesized under different hydrothermal conditions for treatment of hazardous organic pollutants, Particuology 36 (2018) 165-173, doi.org/10.1016/j.partic.2017.05.005.

[47] J. Yu, T. Ma, S. Liu, Enhanced photocatalytic activity of mesoporous TiO_2 aggregates by embedding carbon nanotubes as electron-transfer channel, Phys. Chem. Chem. Phys., 8 (2011) 3491-3501., doi: 10.1039/c0cp01139h

[48] G. Nagaraju, K. Manjunath, S. Sarkar, E. Gunter, Sergio R. Teixeira, J. Dupont, TiO_2–RGO hybrid nanomaterials for enhanced water splitting reaction, Int. J. Hydrog. Energy. 40(36) (2015) 12209-12216. doi.org/10.1016/j.ijhydene.2015.07.094

[49] J.M. Herrmann, Heterogeneous photocatalysis: fundamentals and application to the removal of various types of aqueous pollutants, Catal. Today 53 (1999) 115-129., doi.org/10.1016/S0920-5861(99)00107-8

[50] W.R. Siah, H.O. Lintang, M. Shamsuddin, L. Yuliati, High photocatalytic activity of mixed anatase-rutile phases on commercial TiO_2 nanoparticles, IOP Conf. Ser. Mater. Sci. Eng. 107 (2016) doi: 01200510.1088/1757-899X/107/1/012005

[51] Y. Chen, L. Soler, Ch. Xie, X. Vendrell, J. Serafin, D. Crespo, J. Llorca, A straightforward method to prepare supported Au clusters by mechanochemistry and its application in photocatalysis, Applied Materials Today, 21, (2020), 100873, doi.org/10.1016/j.apmt.2020.100873

[52] C. Xing, Y. Liu, Y. Zhang, J. Liu, T. Zhang, P. Tang, J. Arbiol, L. Soler, K. Sivula, N. Huijarro, X. Wang, J. Li, R. Du, Y. Zao, A. Cabot, J. Llorca, Porous $NiTiO_3/TiO_2$ nanostructures forphotocatatalytic hydrogen evolution, J. Chem. A. , 2018,7, 17053, doi.org/10.1039/C9TA04763H

[53] W. Fan, Q. Lai, Q. Zhang and Y. Wang, nanocomposites of TiO_2 and reduced Graphene Oxide as Efficient Photocatalyst for Hydrogen Evolution, J. Phys. Chem. C, 115 (2011) 10694-10701., doi.org/10.1021/jp2008804

[54] H.-I. Kim, G.-H. Moon, D. Monllor-Satoca, Y. Park and W. Choi, Solar photoconversion Using Graphene/TiO_2 Composites: Nanographene Shell on TiO_2 Core versus TiO_2 Nanoparticles on Graphene Sheet, J. Phys. Chem C, 116 (2012) 1535-1543., doi.org/10.1021/jp209035e

[55] C. Han, Y. Wang, Y. Lei, B. Wang, N. Wu, Q. Shi and Q. Li, In situ synthesis of graphitic-C3N4 nanosheet hybridized N-doped TiO_2 nanofibers for efficient photocatalytic H2 production and degradation, Nano Res., 8 (2015) 1199-1209., doi.org/10.1007/s12274-014-0600-2

[56] J. Gong, C. Yang, J. Zhang and W. Pu, Origin of photocatalytic activity of W/N-codoped TiO_2: H_2 production and DFT calculation with GGA +U, Appl. Cat. B: Environ., 152-153 (2014) 73-81., doi:10.106/j.apcatb.2014.01.028.

[57] L. Kuang, W. Zhang, Enhanced hydrogen Production by carbon-doped TiO_2 Decorated with Reduced Graphene Oxide (rGO) under Visible Light Irradiation, ACS Adv., 6 (2015), doi.org/10.1039/C5RA26096E

[58] X. Zhang, Y. Sun, X. Cui and Z. Jiang, A green and facile synthesis of TiO_2/graphene nanocomposites and their photocatalytic activity for hydrogen evolution, Int. J. Hydrogen Energ., 37 (2012) 811-815., doi.org/10.106/j.ijhydene.2011.04.053.

[59] F. Pei, S. Xu, W. Zuo, Z. Zhang, y. Liu, S. Cao, Effective improvement of photocatalytic hydrogen evolution via a facile in-situ solvothermal N-doping strategy in N-TiO2/N-graphene nanocomposite, 39 (2014(6845-6852., doi.org/10.1016/j.ijhydene.2014.02.173